Journal of Molecular Liquids 359 (2022) 119372

Contents lists available at ScienceDirect

Journal of Molecular Liquids

journal homepage: www.elsevier.com/locate/molliq

Synthesis and characterization of novel blue-emitting nicotinamide-gold nanoclusters with "chain-breaker" antioxidant property

Gyöngyi Gombár [a,b], Ditta Ungor [a,b,*], Gergely F. Samu [b], Orsolya Dömötör [c], Edit Csapó [a,b,*]

[a] MTA-SZTE Lendület "Momentum" Noble Metal Nanostructures Research Group, University of Szeged, H-6720 Rerrich B. sqr. 1, Szeged, Hungary
[b] Interdisciplinary Excellence Center, Department of Physical Chemistry and Materials Science, University of Szeged, H-6720 Rerrich B. sqr. 1, Szeged, Hungary
[c] Department of Inorganic and Analytical Chemistry, University of Szeged, H-6720 Dóm sqr. 7, Szeged, Hungary

ARTICLE INFO

Article history:
Received 1 April 2022
Revised 4 May 2022
Accepted 9 May 2022
Available online 13 May 2022

Keywords:
Nicotinamide
Vitamin B_3 derivative
Gold nanocluster
Antioxidant
ORAC
Chain break

ABSTRACT

In this paper, we firstly demonstrate a simple and reproducible synthesis protocol to produce nicotinamide-stabilized gold nanoclusters (NAM-Au NCs) under mild conditions. The dominant role of the pH and the ligand to metal ion molar ratio on the formation of these few atomic fluorescent NCs were proven. The prepared NCs show intensive blue-emission at 380 nm with two main lifetime components (4.7 and 6.7 ns), which refers to an ultra-small Au NCs structure and nearly uniform composition. The metallic oxidation state of the metal content was identified by X-ray photoelectron spectroscopy, while infrared studies strongly confirm the binding of aromatic-N and the amide-N to the metal core. The oxygen radical capacity (ORAC) tests were carried out in the case of the stabilizing nicotinamide and the prepared NAM-Au NCs using Trolox molecule as reference between 1 and 100 μM concentration range. Based on the fluorometric measurements, we demonstrated that our blue-emitting Au NCs also possess antioxidant activity with 0.48 ± 0.03 Trolox equivalent value. We clearly proved that our sub-nanometer-sized NAM-Au NCs show novel molecular-like optical features against the pure nicotinamide, but the antioxidant effect was also preserved. These coupled properties make our NCs as potential agents for bio-catalytic reactions.

1. Introduction

Nowadays, the discovery of new hybrid materials for different biomedical applications is one of the most interesting research perspectives. Prevention of the oxidative degradation of several organic compounds (*e.g.* lipids, proteins, small drug molecules) is a great challenge in the field of bio-catalysis because atmospheric oxygen can initiate this process by the formation of reactive oxygen species (ROS) [1–3]. Many ways can be utilized, as can be also seen in biological organisms, to inhibit the formation of ROS. However, in this present manuscript, only the "chain break" mechanism is tangentially highlighted due to the examined compounds. During this process, the antioxidant materials can delay or terminate the autooxidation by a formal hydrogen transfer with peroxyl radical in a stoichiometric reaction. The criteria for these "radical-trappers" are (I) the selective and high reactivity against the peroxyl radicals; (II) do not show any spontaneous oxidation process (autoxidation) under air [4]. For this purpose, two types of materials can be used effectively: the inherently, electron-donor antioxidant molecules (*e.g.* phenols [5], ascorbates [6]), or the functionalized nanostructures [7] (*e.g.* CeO_2 [8], Mn_3O_4 nanoparticles (NPs) [9]), which have also electron-rich surfaces. The noble metal-containing NPs or nanoclusters (NCs) are promising structures for this purpose because they have well-defined size- and composition-dependent electric, magnetic, and optical characteristics [10–12]. Moreover, their biological behavior can be easily tuned by the surface ligand and the metal-content [13,14]. It is well-known that the classical noble metal NPs (d > 2 nm), such as gold (Au), silver (Ag), or copper (Cu), show plasmonic properties [15], which can be identified as a characteristic plasmon band on the UV–visible spectra. In contrast, the ultra-small NCs of these elements have molecular-like optical characteristics (photoluminescence (PL)) due to their few-atomic composition [16,17]. In most cases, to ensure desirable PL property, ligand protection of the metal core is necessary [18–21]. The surface-exposed molecules should contain several electron-rich heteroatoms (—NH_2, —COOH, *etc.*) to enhance the ligand-to-metal charge transfer (LMCT) processes between the metal core and stabilizing ligand

* Corresponding authors at: MTA-SZTE Lendület "Momentum" Noble Metal Nanostructures Research Group, University of Szeged, H-6720 Rerrich B. sqr. 1, Szeged, Hungary.
E-mail addresses: ungord@chem.u-szeged.hu (D. Ungor), juhaszne@chem.u-szeged.hu (E. Csapó).

https://doi.org/10.1016/j.molliq.2022.119372
0167-7322/

[22]. Besides, if the heteroatom is sulfur on the metal surface (*e.g.* thiolate ligands), the ligand-to-metal–metal charge transfer (LMMCT) can also realize due to the partially oxidized state of some surface metal atoms [23]. To take these advantages of the applied molecule, besides the optical property, the antioxidant effect of the prepared nano-object can also increase. Based on this fact, there is a growing demand for design of new nanostructures with tunable and unique optical properties, but also with antioxidant features as well. Several colorimetric or fluorometric techniques can be utilized to determine the potential antioxidant effect of the newly synthesized nano-emitters depending on their fluorescent property and the colloid stability [4,24].

The aim of this work is the investigation of the vitamin B_3 derivative named niacinamide or nicotinamide (NAM) as a potential reducing and capping agent for the development of new fluorescent antioxidant Au NCs. This molecule is a well-known nitrogen-containing molecule, which is a bioavailable water-soluble form of vitamin B_3 with antioxidant and anti-inflammatory effects [25]. Firstly, the direct redox reaction between NAM and the tetrachloroaurate ($[AuCl_4]^-$) ions has been investigated in detail to prepare NAM-stabilized Au NCs. The optimization of a reproducible synthetic route is particularly important including but not limited to the study of several important parameters such as the pH-dependent deprotonation of the NAM molecule, the possibility of using an assistant reducing molecule or the synthesis time and temperature *etc*. Besides, the exact structural and optical characterizations of the final product have been carried out by several large-scale techniques. The antioxidant effect of the synthesized nanohybrid structure and the applied surface ligand NAM was also confirmed by the oxygen radical absorbance capacity (ORAC [26,27]) test to get information about the potential multifunction of the synthesized NCs.

2. Experimental

2.1. Materials

Nicotinamide (NAM; $C_6H_6N_2O$; ≥99.5% (HPLC)), hydrogen tetrachloroaurate(III) hydrate ($HAuCl_4{\cdot}H_2O$; 99.9% (metal basis)), 2,2′-azobis (2-methylpropionamidine) dihydrochloride (AAPH; $[{=}NC(CH_3)_2C({=}NH)NH_2]_2 \times 2HCl$; 97%), 6-hydroxy-2,5,7,8-tetramethyl chroman-2-carboxylic acid (Trolox; 97%), trisodium-citrate dihydrate ($C_6H_5Na_3O_7{\cdot}2H_2O$, 99%) were obtained from Sigma-Aldrich. Fluorescein sodium salt (FL; $C_{20}H_{10}Na_2O_5$) was provided from VWR. Sodium hydroxide (NaOH; 99%), hydrochloric acid (HCl; 37%), methanol (CH_3OH; 99.85%), ethanol (C_2H_5OH; 97.0%), sodium chloride (NaCl; 99.98%), sodium-dihydrogen-phosphate 2-hydrate ($NaH_2PO_4{\cdot}2H_2O$; ≥99.9%), disodium hydrogen phosphate dodecahydrate ($Na_2HPO_4{\cdot}12H_2O$; 99.99%) were delivered from Molar Chemicals. All chemical reagents were analytical grade and were used without further purification. The fresh stock solutions were prepared by using Milli-Q ultrapure water (MQ, 18.2 MΩ·cm at 25 °C) in every case.

2.2. Synthesis of NAM-Au NCs

For the synthesis of nicotinamide-stabilized Au NCs (NAM-Au NCs), NAM:$AuCl_4^-$/10:1 M ratio was used, where the final concentration of the Au was 5 mM. As a first step in the synthesis, 278 μL of 0.3 M NAM aqueous solution was added to 1.27 mL of MQ water. After stirring for 2 min, the pH of the reaction mixture was adjusted to pH = 8.0 with 0.1 M NaOH solution, and then 83 μL sodium citrate (c_{final} = 10 mM) and 34 μL of 250 mM $HAuCl_4$ solution were added. After mixing the components, the sample was thermostated at 80 °C ± 1 °C for 24 h. After the synthesis, aggregates were removed by centrifugation at 13000 rpm for 30 min. The final product was purified by dialysis for 180 min using a cellulose tube with 1 kDa cut-off and ultrapure MQ water as dialysis medium at room temperature. The purity of the synthesized NAM-Au NCs was inspected by the measure of metal content, fluorescence signal, and the conductivity of the dialysis medium and cluster suspension.

2.3. Instruments for characterization

During the synthesis, the fluorescence spectra of the NCs were recorded on Horiba Jobin Yvon Fluoromax-4 spectrofluorometer in a 1 cm quartz cuvette using excitation wavelength at 335 nm with a 3 nm slit. The fluorescence lifetime was measured using a Fluoromax spectrofluorometer equipped with a DeltaHub time-correlated single-photon counting (TCSPC) controller using a NanoLED light source N-295 (Horiba Jobin Yvon). The emitted light was detected at λ_{em} = 380 nm with a 3.8 nm slit width and the number of counts on the peak channel was 10,000. The number of channels per curve used for the analysis was *ca.* 1500 with a time calibration of 0.02532 ns/channel. Ludox® (from Sigma-Aldrich) was used as a scatter solution to obtain the instrument response function. Background correction was not needed. The program DAS6 (version 6.6.; Horiba Jobin Yvon) was used for the analysis of the experimental fluorescence decays. The main lifetime components were calculated by the exponentials fitting of decay profile with χ^2 value *ca.* 1. Based on the measured data bi-exponentials fitting was applied with χ^2 = 1.01. The ORAC tests were carried out by using a 1 cm quartz cuvette in a JASCO FP-8500 spectrofluorometer equipped with a JASCO ETC-815 water-cooled Peltier setup. The UV–Vis spectra of the samples were recorded on a JASCO V-770 spectrophotometer with a 1 cm optical length. Infrared spectra of the NCs were measured at room temperature by Jasco FT/IR-4700 in the attenuated total reflectance (ATR) mode between 3500 and 700 cm^{-1}. The resolution was 2 cm^{-1} with 256 scans for all samples. The hydrodynamic diameters and the ζ-potentials were measured with a Zetasizer Nano ZS ZEN 4003 apparatus (Malvern Inst., UK) equipped with a He-Ne laser (λ = 633 nm) at 25 ± 0.1 °C. During the measurements, the hydrodynamic diameters were calculated by ten runs with 2 min/run velocity five times for each sample, and the electrokinetic potential was calculated by the Smoluchowski's formula. The constant ionic strength was I = 0.1 M and regulated by NaCl as inert salt. The X-ray photoelectron spectroscopy (XPS) measurements were done by a SPECS instrument equipped with a PHOIBOS 150MCD9 hemispherical analyzer, under a main-chamber pressure in the 10^{-9}–10^{-10} mbar range. The analyzer was in fixed analyzer transmission mode with 40 eV pass energy for the survey scans and 20 eV pass energy for the high-resolution scans. The sample was deposited on a Pt foil using multistep cyclic lyophilization and loaded into the chamber. The Al Kα X-ray source was used at 200 W power. Charge referencing was done to the 4f peak of the platinum substrate (71.00 eV) on the surface of the sample. For spectrum evaluation, CasaXPS commercial software package was used.

2.4. Measurements of antioxidant effects by ORAC method

During the ORAC method, the PL spectra were registered between 500 and 650 nm each 10 min until the complete disappearance of emission. For analyzes, 485 nm and 515 nm were applied as excitation and emission wavelengths, respectively. The antioxidant capacity (Trolox equivalent) of the synthesized NAM-Au NCs was determined by the following recipe: the adequate volume of antioxidant material suspension/solution and the fluorescein (78 μL of 1 μM) were mixed in phosphate-buffered saline (PBS, c_{NaCl} = 0.15 M, pH = 7.4). The reaction mixture was incubated

in dark for 15 min at 37 °C. The applied concentration range of the examined materials was 1–100 μM (for amide content in the case of NAM-Au NCs). After the resting period, 100 μL of 200 mM AAPH was added to the reaction mixture. Before the measurement, the total volume of the samples was completed with a 2 mL buffer solution for suitable optical signal detection. The Trolox equivalent was calculated by the calibration curves of Trolox, the pure amide, and NAM-Au NCs in the concentration range of 1–100 μM after 20 min reaction time.

3. Results and discussion

3.1. Optimization of one-pot technique for the synthesis of NAM-Au nanohybrid system

As it was mentioned in the *Introduction*, several important parameters are required to be specified for the development of a reproducible synthesis method of a new fluorescent nanomaterial. For this purpose, the effect of the molar ratio between the precursor metal salt and vitamin B_3 derivative was studied firstly on the optical feature of the synthesized product. After mixing the components, where the final concentration of the metal was c_{metal} = 1 mM, the samples were thermostated for 24 h at 25 °C and the fluorescence intensity was checked under UV-lamp (λ_{lamp} = 365 nm). It was observed that the samples have a weak blue fluorescence using the excitation wavelength of the applied lamp. The PL property was characterized by spectrofluorometer as well using λ_{ex} = 335 nm, by which the samples show stronger PL. A typical spectrum series can be seen on Fig. 1A. The experiments have been carried out by using wide molar ratio range (0.1:1–120:1/NAM: $AuCl_4^-$ molar ratio), and it was found that the highest emission maximum is detected at 10:1/ligand:metal ratio (Fig. 1B).

The formation of well-known plasmonic Au NPs with red color was not observed [28]. Thus, for further optimization of the synthesis protocol, this molar ratio was chosen. Beyond the selection of the optimal metal ion to reducing agent ratio, the second important parameter is the initial pH of the ligand solution. It is well-known that the pH has a great influence on the protonation state of the NAM molecule [29,30], and the redox potential also strongly depends on pH. Consequently, the interaction of the ligand molecules with $AuCl_4^-$ ions has been investigated in the initial pH range of 1–12 as Fig. 2A shows. On one hand, the first local maximum of the measured emission is detected at pH 4.0, which is in good agreement with the dominant presence of the deprotonated ligand being charge neutral (dotted line, species B on Fig. 2B) [31]. Based on this, it can be assumed that the deprotonation of the pyridinium ring of the ligand has a great role in the preliminary coordination of the $AuCl_4^-$ ions and the formation of a fluorescent product. On the other hand, it was also observed that the detectable PL shows a 1.6-fold increase at pH = 8.0 than pH = 4.0. To identify this phenomenon the hydrolytic process of the aurate(III) ions should be considered. On Fig. 2B, the distribution of the most dominant complexes (chlorido- and hydroxido-) are also presented (black continuous lines) as a function of pH, which has different redox potential values as well. The three middle fractions having 60–70 M fraction (%) present the different mixed complexes of aurate(III) ($[Au(Cl)_3OH]^-$, $[Au(Cl)_2(OH)_2]^-$, $[AuCl(OH)_3]^-$, respectively).

Based on literature data, in acidic media, the $[AuCl_4]^-$ form is the dominant species and the redox potential is $E_h([AuCl_4]^-/Au^0)$ = 1.00 V. In contrast, the $[Au(OH)_4]^-$ complex becomes the main form at pH 8.0 with $E_h([Au(OH)_4]^-/Au^0)$ = 0.60 V. Thus, in the alkaline pH range, not only the increased reducing capacity and coordination tendency of the pyridine containing molecule [32–34] promotes the cluster formation, but the total reduction of gold from ionic to metallic form becomes also preferable due to the lower redox potential of the dominant gold complex. For this ligand, the value of the redox potential at pH = 4.0 and pH = 8.0 is nearly the same, because no structural change occurred with the molecule above pH = 4.0. If the pH reaches the pH = 9.0 a slight decrease in the PL intensity is observed; most probably the stability of the fluorescent product is decreased. To promote the total reduction of the precursor metal ions and to increase of yield of the fluorescent gold products, the absence, and presence of sodium citrate as an assistant mild reducing agent were also examined. As it can be seen on Fig. 3A the limited use of citrate further aids the reaction because the PL intensity was increased. Although, the Turkevich-method [28] is well-known to produce colloidal Au particles using only sodium citrate as a reducing agent at boiling temperature (*ca.* 100 °C). In contrast, the plasmonic NPs formation is avoided due to the presence of NAM in the presented synthesis. To investigate the effect of the citrate concentration, it was determined that the ideal amount is 10 mM ($AuCl_4^-$:citrate/ 1:2 M ratio), which can suitably support the formation of the blue-emitting NAM-Au nanohybrid product to a greater extent. If we further increase the amount of citrate the PL intensity values show decreasing tendency, and in case of extreme citrate excess (c > 100 mM), PL intensity starts to increase again. Most probably the formation of few-atomic metallic clusters seeds is unfavorable if the Au/citrate ratio exceeds the 1:5 ratio in presence of nicotinamide perhaps due to the excessive separation of the reduced

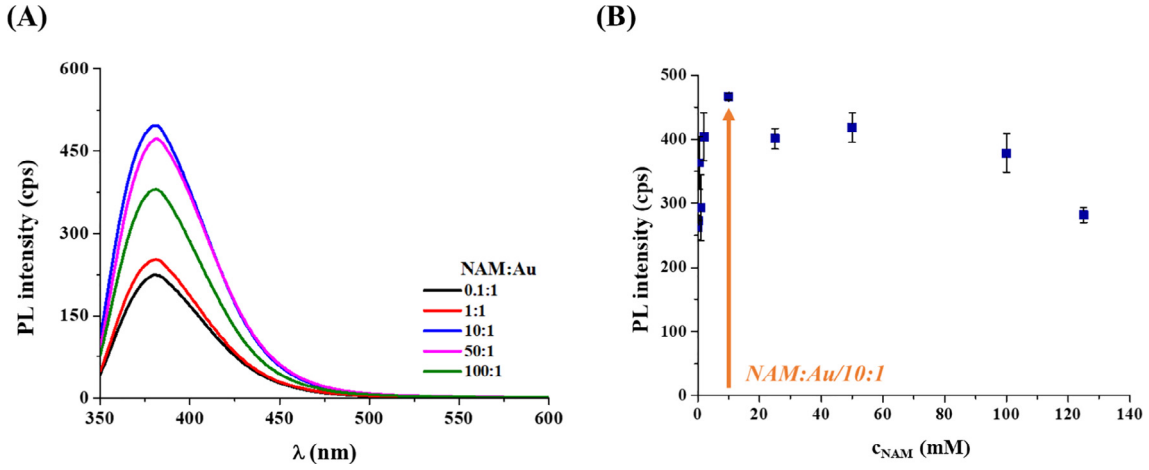

Fig. 1. A representative spectrum series of the final fluorescent product after 24 h using different molar ratios of NAM and $AuCl_4^-$ ions **(A)**. The maxima of the measured average emission intensity at λ_{em} = 380 nm depending on the NAM concentration (c_{Au} = 1 mM, λ_{ex} = 335 nm) **(B)**.

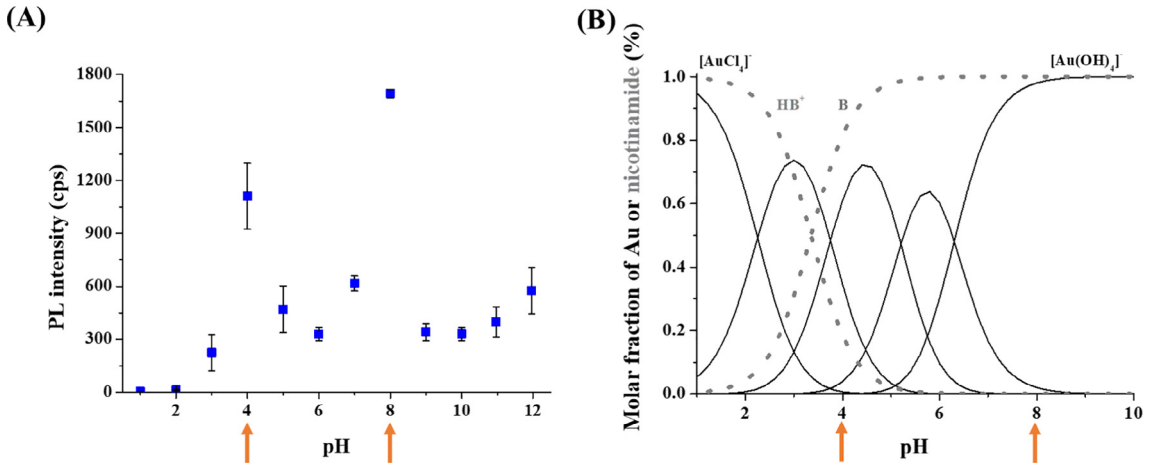

Fig. 2. The measured emission intensity of the product (λ_{em} = 380 nm) as a function of the initial pH of the reaction mixture **(A)**. Concentration distribution curves of the NAM molecule (dotted lines) and the dominant chlorido and hydroxido complexes of the aurate(III) ions (solid lines) depending on the pH **(B)**. (c_{Au} = 1 mM, c_{NAM} = 10 mM, λ_{ex} = 335 nm).

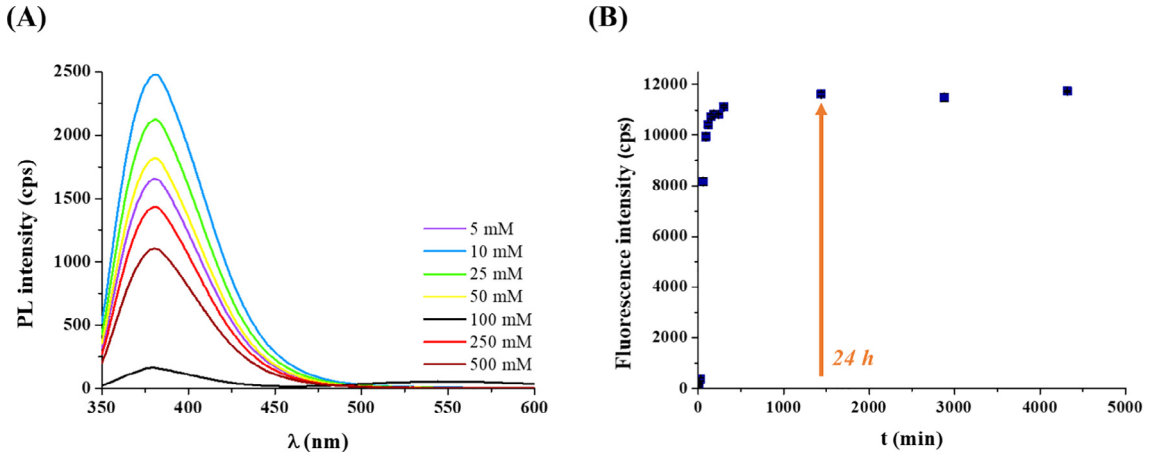

Fig. 3. The measured PL spectra of the final products using different citrate concentrations (c_{Au} = 1 mM, c_{NAM} = 10 mM, λ_{ex} = 335 nm, initial pH = 8.0, T = 80 °C) **(A)**. The measured PL intensity values of the products as a function of the time using the optimized parameters (c_{Au} = 5 mM, c_{NAM} = 50 mM, λ_{ex} = 335 nm, λ_{em} = 380 nm, initial pH = 8.0, T = 80 °C) **(B)**.

metal atoms, which inhibits the cluster formation. For random change of the PL intensity using extreme citrate excess (c > 100 mM) we do not yet have an answer that can be supported by experimental results, perhaps complex formation or other interaction between the ligands can be occurred.

Finally, three more parameters were also optimized, while the previously defined parameters were kept constant: the metal concentration (**Fig. S1A**), the temperature (**Fig. S1B**), and the synthesis time (Fig. 3B). These key conditions also have a great influence on the amount, chemical structure, and optical properties of the formed nanohybrid systems. Based on the experiments, the ideal metal concentration is 5.0 mM to produce NAM-Au fluorescence products having great PL. The use of smaller metal content causes lower PL, but in contrast, if the precursor metal salt concentration reaches ~ 5.0 mM, large aggregates are formed and the rapid association of the luminescent adducts is observed. For temperature, it was found that the continuous increase in temperature from 25 °C to 80 °C is increasingly favorable for the formation of clusters, but negligible PL is detectable at lower temperatures (*e.g.* 4 °C). The most amount of the luminescent nano-object can be formed using 80 °C. Finally, the exact synthesis time was determined based on the measurement of time-dependent fluorescence evolution, which is 24 h under the use of the optimized parameters. The final product was purified in a two-step process as described in the *Experimental (chapter 2.2)* section.

3.2. Structural characterization of the fluorescent NAM-Au NCs

For the characterization of the synthesized blue-emitting objects with optimized parameters, the optical properties were determined first. As it can be seen on Fig. 4A, the prepared NAM-Au NCs show intensive blue emission. Based on the detected well-defined excitation and emission spectra with relatively small Stokes shift (*ca.* 45 nm), maxima can be identified at 335 and 380 nm, respectively.

Based on the literature data, the blue-emitting gold-based objects can show diverse chemical structures [16]. These materials can be supramolecular complexes [35–38], where the central metallic component shows an ionic form with a + 1 oxidation state in most cases, and the ligand contains 'P' or 'S' donor atoms. Using small biomolecule having nitrogen-rich functional group(s) as a direct reducing agent, polynuclear complexes with ionic metal centers or few-atomic Au NCs having metallic cores can also be formed depending on the reduction capacity of the ligand [18]. Naturally, the presence of other assistant reducing agents, such as sodium borohydride, citrate, hydrazine, or the change of the initial pH

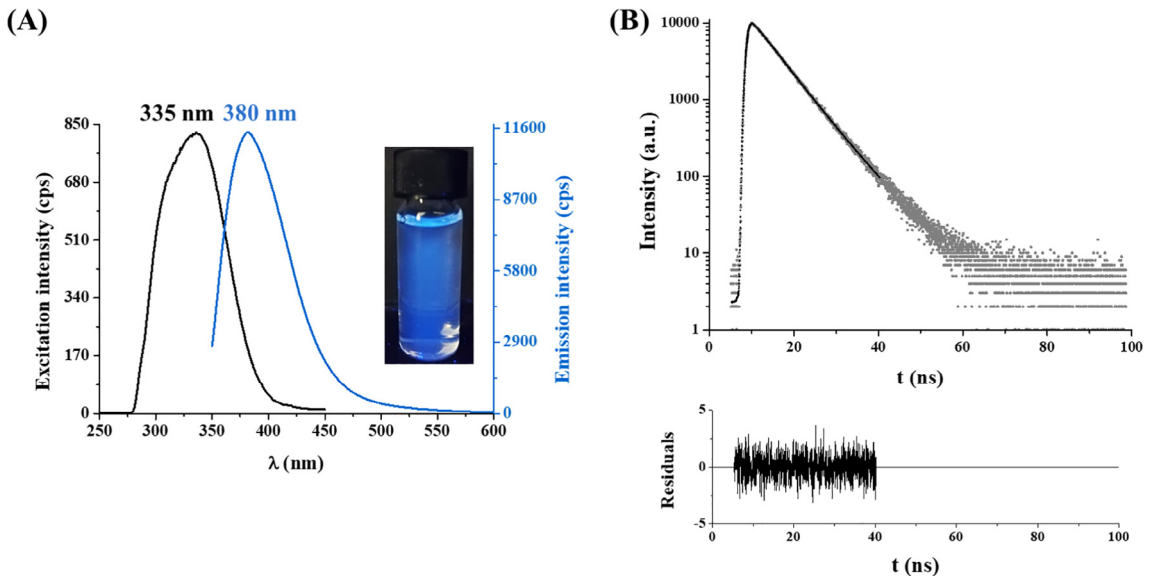

Fig. 4. The excitation and emission spectra of the NAM-Au system with the photo of the sample under UV-lamp (c_{Au} = 5 mM, λ_{lamp} = 365 nm) **(A)**. Measured (gray dots) and fitted (black line) fluorescence decay curves of the blue-emitting nano-object (λ_{ex} = 295 nm, λ_{em} = 380 nm) **(B)**. (For interpretation of the references to color in this figure legend, the reader is referred to the web version of this article.)

can enhance the formation of ultra-small metallic NCs [39–41]. Besides, the steady-state measurements, the time-correlated single-photon counting (TCSPC) technique is a reliable method to estimate the structure, as well as the oxidation state of the produced Au-containing quantum dots [16]. After the evaluation of the decay curve (Fig. 4B), two fluorescent lifetime (τ) components were identified: τ_1 = 4.3 ns (amplitude: α_1 = 32%) and τ_2 = 6.7 ns (α_2 = 68%). It is generally accepted that the emission and the τ values of the ultra-small Au NCs are dependent dominantly on the atom number in the cluster core and the chemical structure of the stabilizing ligand [42]. The determined fluorescence parameters of the synthesized NAM-Au system are in good agreement with the work of M. Dickson and co-workers [41]. Their work focuses on the tunable preparation of poly(amidoamine) (PAMAM) dendrimer-stabilized Au NCs having size-dependent fluorescence. Besides, it was found that the synthesized NCs exhibited nanosecond-scale luminescence lifetimes during, the short Stokes shift. A good correlation was also identified between the value of the atoms in the cluster core and emission energies in the case of Au_5–Au_{31} ultra-small Au NCs. In their paper, they concluded that the luminescence dominantly originates from the metal core of Au NCs instead of the ligand to metal charge transfer (LMCT). Thus, the excitation and emission energies are well described by the free electron Jellium model. Based on our measured data, it can be assumed that the prepared NAM-Au NCs have almost analogous cluster structure to the PAMAM-Au NCs synthesized by M Dickson Group due to the similar donor groups of both stabilizing ligands. Based on these conclusions, the fluorescence of the prepared NAM-Au NCs origins presumably from the protoplasmonic sp-sp intraband electron transition [43] of the metallic cluster cores. Besides, the difference between the measured τ components is a rather small value, which also refers the nearly uniform size composition.

To verify the metallic nature of the atoms in the NCs, the XPS measurement was carried out (Fig. 5A). In the bulk phase, the 4f electrons of the Au have Au $4f_{7/2}$–84.0 eV binding energy (BE) [44]. It is well-known that this BE is extremely sensitive to both the oxidation state of the Au, the size of the metal (particle), as well as the strength of the interaction with the surface ligand [45]. Fig. 5A shows that the measured BEs are 87.5 and 83.8 eV in the case of $4f_{5/2}$ and $4f_{7/2}$, respectively. These values refer to the 'zero' oxidation state of the Au in the cluster cores, which confirms the metallic behavior of these fluorescent nano-objects. The negative shift compared to the bulk energies also refers to the ultra-small core size. Moreover, the strong interaction between vitamin B_3 derivative and Au NCs is also supported.

In general, the amide and pyridine nitrogen energies are located at 399.7 and 399.5 eV, respectively [46]. Based on the XPS spectra of the 'N' atoms (**Fig. S2**) in the NAM-Au NCs, it can be concluded that the N 1s region can be fitted with one component. In this sample, the 1s BE is located at 400.1 eV, which refers to a strong bond between the ligand and metal cores. Furthermore, even both types of nitrogen can take part in the stabilization of the metal core.

The FT-IR studies are one of the best techniques to analyze the conformation or structural changes of the applied ligand before and after the metal particle synthesis. Based on the registered spectra, the moieties, which take part in the stabilization of the formed "colloidal" system, and the free groups can be also identified. As it can be read in *chapter 3.1*, it was concluded that the preliminary coordination of the precursor metal ion possibly occurs through the pyridine-nitrogen based on the pH-dependent synthesis. Besides, on the IR spectra (Fig. 5B), it also can be concluded that the amide group of the ligand has a great role in the stabilization process of the few-atomic Au NCs presumably due to metal ion-induced amide deprotonation. Namely, the symmetric (ν_s) and asymmetric (ν_{as}) stretching of the (NH_2) group is changed from 3365 and 3156 cm^{-1} to 3358 and 3149 cm^{-1} for NAM and NAM-Au NCs, respectively [47]. Besides, the stretching vibration (ν) of the pyridine ring also changes drastically from 1569 cm^{-1} to 1574 cm^{-1}. The other moieties and atomic groups of the ligand are invariable after the metal coordination.

Last, the aggregation tendency was investigated in various media using three different parameters. For this purpose, the optical property (Fig. 6A), the change of the hydrodynamic diameter (d_H), as well as the ζ-potential (Fig. 6B) were measured depending on the pH at 25 °C. The constant ionic strength was regulated by the presence of sodium chloride as inert salt. Fig. 6A clearly shows that the fluorescence of the synthesized NCs is detectable in the whole studied pH region (pH = 1.0–12.0) but between pH = 1.0–3.0 and above pH = 10.0 a slight decrease can be observed. Under

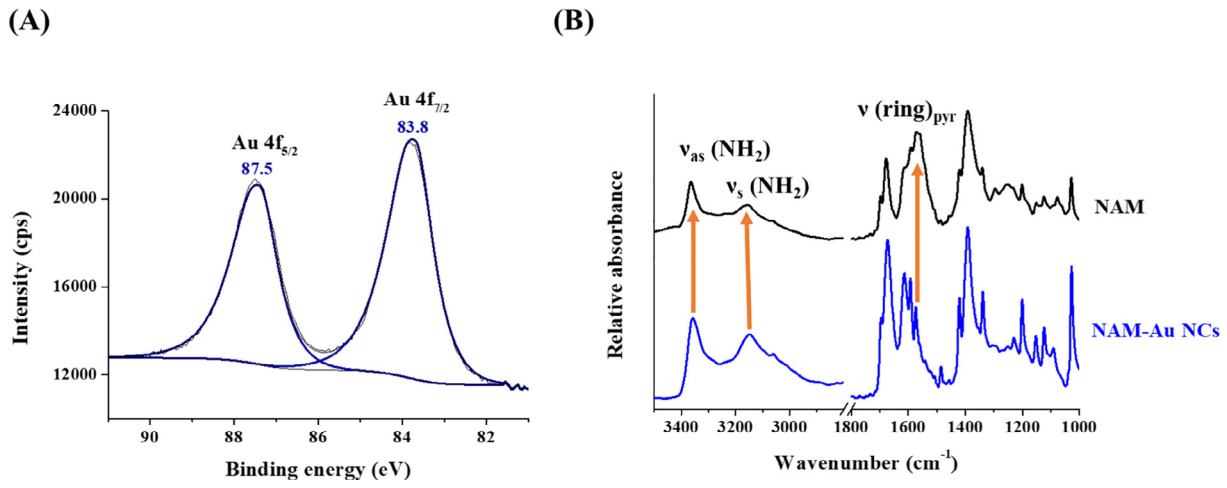

Fig. 5. XPS spectrum of the gold in the NAM-Au NCs **(A)**. The FT-IR spectra of the pure ligand (upper) and the NAM-Au NCs (lower) **(B)**.

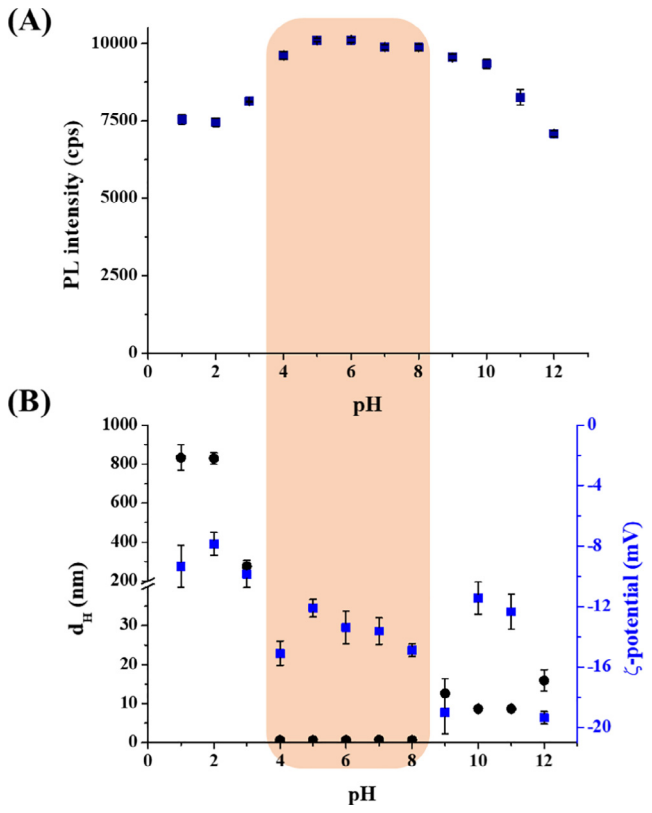

Fig. 6. Emission intensities (λ_{em} = 380 nm, λ_{ex} = 335 nm) of NAM-Au NCs depending on the pH **(A)**. The measured hydrodynamic diameters (●) and ζ-potential values (■) as a function of pH (T = 25 °C, I = 0.1 M) **(B)**.

strong acidic conditions (1.0 < pH < 3.0), large aggregates are formed (d_H > 800 nm), and the ζ-potential values refer to the metastable state of the NAM-Au NCs [48]. In contrast, if the clusters are under mild conditions (pH = 5.0–8.0) dominant changes in the fluorescence cannot be observed.

Although the measured hydrodynamic diameters ($d_H \sim 1$ nm) are close to the detection limit of the instrument, the ultra-small Au NCs cannot show any aggregation process. The magnitude of the ζ-potential values also confirms the more stable region of this system between pH = 4.0–8.0 [48]. Considering the more alkali conditions, if the pH is higher than pH = 9.0, the clusters lose their stability again thanks to the high electrostatic shielding. The fluorescence decreases moderately, moreover, the size also increased to *ca.* 10–15 nm.

3.3. Determining the oxygen radical absorbance capacity (ORAC)

As it was mentioned in the *Introduction*, the chosen stabilizing molecule (vitamin B_3 derivative NAM) has a great antioxidant and anti-inflammatory effect [25]. For the correct determination of the antioxidant effect, it should be considered both the optical property and colloid stability of the prepared NAM-Au NCs. Based on the results of the characterization, the chosen method is the ORAC test [4], which has several advantages such as the biological relevant free radical and standardized methodology. During this reaction, the decay curve of the fluorescein dye is measured in the presence and absence of antioxidant molecules after the reaction of the ROS. The reactive peroxyl radical is represented by thermolytic decomposition of a hydrophilic azo-containing molecule (AAPH), which can destroy the dye molecule resulting the decrease of fluorescence signal [49]. The measurements are usually carried out in two independent ways: (I) measure the time-dependent signal loss of fluorescence with constant antioxidant concentration; (II) measure the fluorescence intensities at the same reaction time using different concentration of antioxidant. To standardize the measured values, the hydrophilic vitamin E analog molecule (Trolox) is generally accepted.

To utilize the antioxidant advantage, the inhibition capacity of the synthesized NAM-Au NCs on the fluorescein degradation was measured by the above-detailed spectrofluorimetric ORAC method [26,27]. Besides, the antioxidant effect of the pure NAM was also measured, and the result was compared with the poor literature data.

The registered PL signals can be seen on Fig. 7. As it can be seen on **Fig. S3A**, the characteristics of the Trolox curves are similar to the literature data. It can be concluded that the larger concentration of vitamin E derivate can successfully inhibit the dye degradation. Based on **Fig. S3B**, it can be also established that the NAM content is less able to prevent the ROS formation as expected. However, it can be concluded based on the measurement data that the Au content with a smaller NAM concentration can slightly prevent the dye from degradation (Fig. 7B), which is proven by the prolonged duration of the registered signal. It should be also mentioned that if the vitamin concentration reaches 100 μM, the pure NAM has the more dominant antioxidant effect. Besides the analysis of the fluorescence signal characteristic, the Trolox equivalent

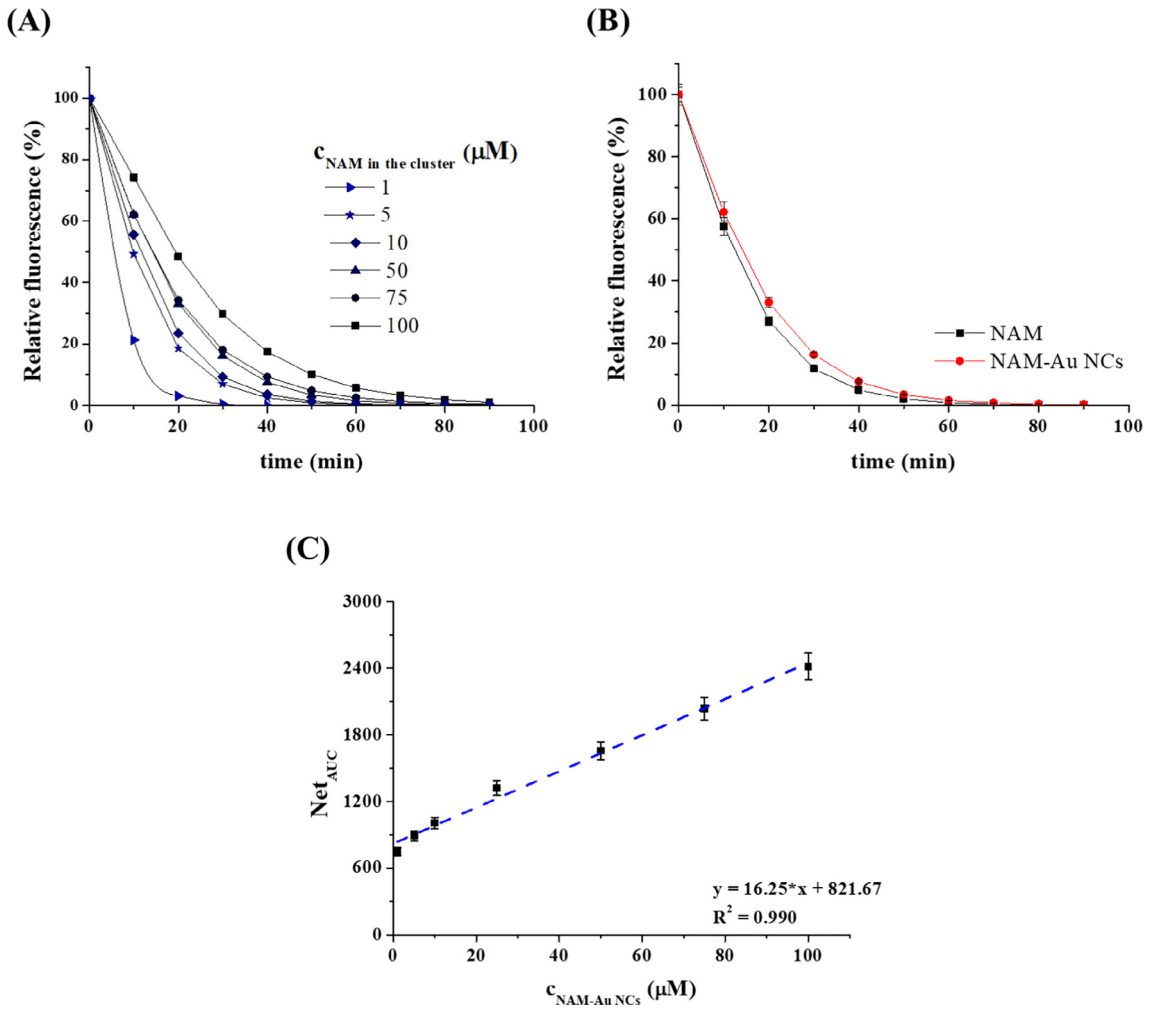

Fig. 7. Representative signal curves of the fluorescein dye at λ_{em} = 515 nm for different NAM-Au NCs (in terms of the amount of NAM) concentration as a function of time (T = 37 °C) **(A)**. Comparison of the PL signals of pure NAM and Au NCs (c_{NAM} = 50 μM) **(B)**. The ORAC calibration curve of the NAM-Au NCs between 1 and 100 μM **(C)**.

(TE) or ORAC value of the examined materials to 1 μM Trolox was also calculated. For this purpose, the net area under curve (Net_{AUC}) values (Fig. 7C) needed to be determined by integration of the time-dependent curves (Fig. 7A and Fig. S3) using blank samples without antioxidant compounds [50].

Based on calculated data the ORAC value [51]:

$$ORAC\,value = \frac{c_{Trolox} * Net_{AUCofsample} * k}{Net_{AUCofTrolox}} \quad (1)$$

where the c_{Trolox} is the standardized concentration of Trolox (50 μM), the Net_{AUC} of the sample at 50 μM NAM concentration, and Net_{AUC} of Trolox is the net area under decay curves in the case of the NAM and NAM-Au NCs samples and Trolox, respectively. The k is the dilution factor of the sample. In the applied method, the dilution factor was 4.3.

The measured samples show weaker antioxidant activity than the standard Trolox molecule, as Table 1 shows. However, the NAM-Au NCs have a smaller TE value perhaps due to metal-attached active moieties. Nonetheless, their antioxidant property shows a delaying effect on the dye degradation and takes better activity against the synthetic vitamin mixture and tannic acid. Considering the chemical structure of the NAM molecule, as it was mentioned in the Introduction the hypothesized "chain-break" mechanism is confirmed by the ORAC test.

Table 1
The TE antioxidant capacity of different compounds by the ORAC method.

Material	Concentration (μM)	TE	Ref.
Nicotinamide	50	0.56 ± 0.02	Presented
Nicotinamide-Au NCs	50*	0.48 ± 0.03	Presented
Tannic acid	8.8×10^{-3}	0.23 ± 0.02	[50]
Uric acid	0–4	1.08	[51]
Ascorbic acid	0–2	1.9	[51]
Vitamin B_3 in synthetic B vitamin Mixture	44.7	0.28	[52]

* In terms of the amount of NAM.

4. Conclusion

In this paper, a simple one-pot synthesis was presented to produce blue-emitting NAM-Au NCs. For stabilization, the non-studied amide derivate of vitamin B_3 molecule (NAM) was chosen, which coordinates the metal cores via the pyridine and amide functions. The optical features show intensive light emission at 380 nm and the determined lifetime values refer to the nearly uniform size of few-atomic Au NCs. The oxidation state of the metal content was analyzed by XPS, and the zero valency binding energies were identified at $4f_{5/2}$ = 87.5 eV and $4f_{7/2}$ = 83.8 eV. The antioxidant effect of the NAM, as well as the NAM-Au NCs, was measured by the ORAC

method and the Trolox equivalent value was calculated to analyze their inhibition capacity against ROS generation. The initial antioxidant effect was kept after the metal coordination but slightly decreased due to the metal-coordinated active functional groups. The pure vitamin derivative has 0.56 ± 0.02, while the NAM-Au NCs show 0.48 ± 0.03 TE related to 1 μM Trolox concentration. They have a moderate prolonged effect on dye degradation at the same concentration. We clearly demonstrated that our sub-nanometer-sized NAM-Au NCs show new molecular-like blue fluorescence in contrast to the pure molecule, but the antioxidant capacity remains similar. These coupled properties make our NCs as potential agents for biocatalytic reactions.

CRediT authorship contribution statement

Gyöngyi Gombár: Methodology, Investigation, Writing – original draft. **Ditta Ungor:** Methodology, Investigation, Visualization, Writing – original draft. **Gergely F. Samu:** Investigation. **Orsolya Dömötör:** Investigation. **Edit Csapó:** Conceptualization, Writing – original draft, Writing – review & editing, Supervision, Resources.

Declaration of Competing Interest

The authors declare that they have no known competing financial interests or personal relationships that could have appeared to influence the work reported in this paper.

Acknowledgment

Project no. TKP2021-EGA-32 has been implemented with the support provided by the Ministry of Innovation and Technology of Hungary from the National Research, Development and Innovation Found, financed under the TKP2021-EGA funding scheme. The research was supported by NRDI Office–"OTKA" FK 131446 and PD 137938 projects. The authors thank the possibility of János Bolyai Research Fellowship of the Hungarian Academy of Sciences. The publication was also funded by the University of Szeged Open Access Fund (FundRef, Grant No. 5738).

Appendix A. Supplementary material

Supplementary data to this article can be found online at https://doi.org/10.1016/j.molliq.2022.119372.

References

[1] J. Morry, W. Ngamcherdtrakul, W. Yantasee, Oxidative stress in cancer and fibrosis: opportunity for therapeutic intervention with antioxidant compounds, enzymes, and nanoparticles, Redox Biol. 11 (2017) 240–253, https://doi.org/10.1016/j.redox.2016.12.011.
[2] L. Valgimigli, A. Baschieri, R. Amorati, Antioxidant activity of nanomaterials, J. Mater. Chem. B. 6 (2018) 2036–2051, https://doi.org/10.1039/c8tb00107c.
[3] S. Muráth, N.B. Alsharif, S. Sáringer, B. Katana, Z. Somosi, I. Szilagyi, Antioxidant materials based on 2d nanostructures: a review on recent progresses, Crystals. 10 (2020) 40–49, https://doi.org/10.3390/cryst10030148.
[4] I.G. Munteanu, C. Apetrei, Analytical methods used in determining antioxidant activity: a review, Int. J. Mol. Sci. 22 (2021), https://doi.org/10.3390/ijms22073380.
[5] C.A. Rice-Evans, N.J. Miller, G. Paganga, Antioxidant properties of phenolic compounds, Trends Plant Sci. 2 (1997) 152–159, https://doi.org/10.1016/S1360-1385(97)01018-2.
[6] R.E. Beyer, The role of ascorbate in antioxidant protection of biomembranes: interaction with vitamin E and coenzyme Q, J. Bioenerg. Biomembr. 26 (1994) 349–358, https://doi.org/10.1007/BF00762775.
[7] M. Wojnicki, V. Hessel, Quantum materials made in microfluidics - critical review and perspective, Chem. Eng. J. 438 (2022) 135616, https://doi.org/10.1016/j.cej.2022.135616.
[8] B. Nelson, M. Johnson, M. Walker, K. Riley, C. Sims, Antioxidant cerium oxide nanoparticles in biology and medicine, Antioxidants 5 (2016) 15, https://doi.org/10.3390/antiox5020015.
[9] N. Singh, M.A. Savanur, S. Srivastava, P. D'Silva, G. Mugesh, A redox modulatory Mn3O4 nanozyme with multi-enzyme activity provides efficient cytoprotection to human cells in a Parkinson's disease model, Angew. Chem. – Int. Ed. 56 (2017) 14267–14271, https://doi.org/10.1002/anie.201708573.
[10] D. Mott, J.D. Lee, N.T.B. Thuy, Y. Aoki, P. Singh, S. Maenosono, A study on the plasmonic properties of silver core gold shell nanoparticles: optical assessment of the particle structure, Jpn. J. Appl. Phys. 50 (2011), https://doi.org/10.1143/JJAP.50.065004.
[11] Q.Q. Xu, X.Y. Dong, R.W. Huang, B. Li, S.Q. Zang, T.C.W. Mak, A thermochromic silver nanocluster exhibiting dual emission character, Nanoscale 7 (2015) 1650–1654, https://doi.org/10.1039/c4nr05122j.
[12] D. Ungor, Csapó, reduction of tetrachloroaurate(III) ions with bioligands: role of the thiol and amine functional groups on the structure and optical features of gold nanohybrid systems, Nanomaterials 9 (2019) 1229, https://doi.org/10.3390/nano9091229.
[13] Y. Liu, Y. Qing, L. Jing, W. Zou, R. Guo, Platinum-copper bimetallic colloid nanoparticle cluster nanozymes with multiple enzyme-like activities for scavenging reactive oxygen species, Langmuir 37 (2021) 7364–7372, https://doi.org/10.1021/acs.langmuir.1c00697.
[14] A. Czyżowska, A. Barbasz, L. Szyk-Warszyńska, M. Oćwieja, E. Csapó, D. Ungor, The surface-dependent biological effect of protein-gold nanoclusters on human immune system mimetic cells, Colloid. Surf. A Physicochem. Eng. Asp. 620 (2021) 126569, https://doi.org/10.1016/j.colsurfa.2021.126569.
[15] X. Huang, M.A. El-Sayed, Gold nanoparticles: optical properties and implementations in cancer diagnosis and photothermal therapy, J. Adv. Res. 1 (2010) 13–28, https://doi.org/10.1016/j.jare.2010.02.002.
[16] J. Zheng, C. Zhou, M. Yu, J. Liu, Different sized luminescent gold nanoparticles, Nanoscale 4 (2012) 4073, https://doi.org/10.1039/c2nr31192e.
[17] M. Zhou, C. Zeng, Q. Li, T. Higaki, R. Jin, Gold nanoclusters: Bridging gold complexes and plasmonic nanoparticles in photophysical properties, Nanomaterials 9 (2019), https://doi.org/10.3390/nano9070933.
[18] E. Csapó, D. Ungor, Z. Kele, P. Baranyai, A. Deák, Á. Juhász, L. Janovák, I. Dékány, Influence of pH and aurate/amino acid ratios on the tuneable optical features of gold nanoparticles and nanoclusters, Colloids Surfaces A Physicochem. Eng. Asp. 532 (2017) 601–608, https://doi.org/10.1016/j.colsurfa.2017.02.047.
[19] D. Ungor, E. Csapó, B. Kismárton, Á. Juhász, I. Dékány, Nucleotide-directed syntheses of gold nanohybrid systems with structure-dependent optical features: selective fluorescence sensing of Fe^{3+} ions, Colloids Surf. B Biointerf. 155 (2017) 135–141, https://doi.org/10.1016/j.colsurfb.2017.04.013.
[20] D. Ungor, K. Horváth, I. Dékány, E. Csapó, Red-emitting gold nanoclusters for rapid fluorescence sensing of tryptophan metabolites, Sens. Actuat., B Chem. 288 (2019) 728–733, https://doi.org/10.1016/j.snb.2019.03.026.
[21] D. Ungor, I. Szilágyi, E. Csapó, Yellow-emitting Au/Ag bimetallic nanoclusters with high photostability for detection of folic acid, J. Mol. Liq. 338 (2021), https://doi.org/10.1016/j.molliq.2021.116695 116695.
[22] T.Q. Yang, B. Peng, B.Q. Shan, Y.X. Zong, J.G. Jiang, P. Wu, K. Zhang, Origin of the photoluminescence of metal nanoclusters: from metal-centered emission to ligand-centered emission, Nanomaterials 10 (2020) 1–24, https://doi.org/10.3390/nano10020261.
[23] K. Pyo, V.D. Thanthirige, K. Kwak, P. Pandurangan, G. Ramakrishna, D. Lee, Ultrabright luminescence from gold nanoclusters: rigidifying the Au(I)-thiolate shell, J. Am. Chem. Soc. 137 (2015) 8244–8250, https://doi.org/10.1021/jacs.5b04210.
[24] B. Khlebtsov, A. Prilepskii, M. Lomova, N. Khlebtsov, Au-nanocluster-loaded human serum albumin nanoparticles with enhanced cellular uptake for fluorescent imaging, J. Innov. Opt. Health Sci. 9 (2016) 1–8, https://doi.org/10.1142/S1793545816500048.
[25] M. Lappas, M. Permezel, The anti-inflammatory and antioxidative effects of nicotinamide, a vitamin B_3 derivative, are elicited by FoxO3 in human gestational tissues: implications for preterm birth, J. Nutr. Biochem. 22 (2011) 1195–1201, https://doi.org/10.1016/j.jnutbio.2010.10.009.
[26] A. Zulueta, M.J. Esteve, A. Frígola, ORAC and TEAC assays comparison to measure the antioxidant capacity of food products, Food Chem. 114 (2009) 310–316, https://doi.org/10.1016/j.foodchem.2008.09.033.
[27] M.K. Roy, M. Koide, T.P. Rao, T. Okubo, Y. Ogasawara, L.R. Juneja, ORAC and DPPH assay comparison to assess antioxidant capacity of tea infusions: relationship between total polyphenol and individual catechin content, Int. J. Food Sci. Nutr. 61 (2010) 109–124, https://doi.org/10.3109/09637480903292601.
[28] J. Turkevich, P.C. Stevenson, J. Hillier, P.H.J. Turkevich, John Cooper, A study of the nucleation and growth processes in the synthesis of colloidal gold, Discuss. Faraday Soc. 11 (1951) 55, https://doi.org/10.1039/df9511100055.
[29] H.H.G. Jellinek, M.G. Wayne, Nicotinamide. Ultraviolet Absorption Spectra and Dissociation Constants, J. Phys. Chem. 55 (1951) 173–180. doi:10.1021/j150485a002.
[30] B. Birdsall, J. Feeney, P. Partington, Ionisation, self association, and proton exchange studies of nicotinamide in aqueous solution using nuclear magnetic resonance spectroscopy, J. Chem. Soc. Perkin Trans. 2 (1973) 2145, https://doi.org/10.1039/p29730002145.
[31] A. Jaworska, K. Malek, K.M. Marzec, M. Baranska, Nicotinamide and trigonelline studied with surface-enhanced FT-Raman spectroscopy, Vib. Spectrosc. 63 (2012) 469–476, https://doi.org/10.1016/j.vibspec.2012.09.004.
[32] R. Rellán-Álvarez, J. Abadía, A. Álvarez-Fernández, Formation of metal-nicotianamine complexes as affected by pH, ligand exchange with citrate and metal exchange. A study by electrospray ionization time-of-flight mass spectrometry, Rapid Commun. Mass Spectrom. 22 (2008) 1553–1562, https://doi.org/10.1002/rcm.3523.

[33] A.J. Lucio, S.K. Shaw, Pyridine and pyridinium electrochemistry on polycrystalline gold electrodes and implications for CO2 reduction, J. Phys. Chem. C. 119 (2015) 12523–12530, https://doi.org/10.1021/acs.jpcc.5b03355.
[34] M.D. Lovander, J.D. Lyon, D.L. Parr, J. Wang, B. Parke, J. Leddy, Critical review—electrochemical properties of 13 vitamins: a critical review and assessment, J. Electrochem. Soc. 165 (2) (2018) G18–G49.
[35] F. Scherbaum, A. Grohmann, B. Huber, C. Krüger, H. Schmidbaur, "Aurophilicity" as a consequence of relativistic effects: the hexakis (triphenylphosphaneaurio)methane dication $[(Ph_3PAu)_6C]^{2\oplus}$, Angew. Chem. Int. Ed. English. 27 (1988) 1544–1546, https://doi.org/10.1002/anie.198815441.
[36] V. Balzani, A. Juris, M. Venturi, S. Campagna, S. Serroni, Luminescent and redox-active polynuclear transition metal complexes †, Chem. Rev. 96 (1996) 759–834, https://doi.org/10.1021/cr941154y.
[37] Z. Assefa, J.M. Forward, T.A. Grant, R.J. Staples, B.E. Hanson, A.A. Mohamed, J.P. Fackler, Three-coordinate, luminescent, water-soluble gold(I) phosphine complexes: structural characterization and photoluminescence properties in aqueous solution, Inorg. Chim. Acta. 352 (2003) 31–45, https://doi.org/10.1016/S0020-1693(03)00134-8.
[38] C. Latouche, Y.R. Lin, Y. Tobon, E. Furet, J.Y. Saillard, C.W. Liu, A. Boucekkine, Au-Au chemical bonding induced by UV irradiation of dinuclear gold(I) complexes: a computational study with experimental evidence, Phys. Chem. Chem. Phys. 16 (2014) 25840–25845, https://doi.org/10.1039/c4cp03990d.
[39] T.G. Schaaff, G. Knight, M.N. Shafigullin, R.F. Borkman, R.L. Whetten, Isolation and selected properties of a 10.4 kDa gold: glutathione cluster compound, J. Phys. Chem. B. 102 (1998) 10643–10646, https://doi.org/10.1021/jp9830528.
[40] T.G. Schaaff, R.L. Whetten, Giant gold−glutathione cluster compounds: intense optical activity in metal-based transitions, J. Phys. Chem. B. 104 (2000) 2630–2641, https://doi.org/10.1021/jp993691y.
[41] J. Zheng, C. Zhang, R.M. Dickson, Highly fluorescent, water-soluble, size-tunable gold quantum dots, Phys. Rev. Lett. 93 (2004) 077402, https://doi.org/10.1103/PhysRevLett.93.077402.
[42] Y. Huang, L. Fuksman, J. Zheng, Luminescence mechanisms of ultrasmall gold nanoparticles, Dalt. Trans. 47 (2018) 6267–6273, https://doi.org/10.1039/c8dt00420j.
[43] J. Zheng, P.R. Nicovich, R.M. Dickson, Highly fluorescent noble-metal quantum dots, Annu. Rev. Phys. Chem. 58 (2007) 409–431, https://doi.org/10.1146/annurev.physchem.58.032806.104546.
[44] M. Wojnicki, B. Michorczyk, K. Wojtaszek, D. Kutyła, K. Kołczyk-Siedlecka, S. Małecki, A. Wrzesińska, M. Kozanecki, P. Kwolek, M. Gajewska, R.P. Socha, E. Csapó, M. Escribà-Gelonch, V. Hessel, Zero waste, single step methods of fabrication of reduced graphene oxide decorated with gold nanoparticles, Sustain. Mater. Technol. 31 (2022) e00387.
[45] S. Peters, S. Peredkov, M. Neeb, W. Eberhardt, M. Al-Hada, Size-dependent XPS spectra of small supported Au-clusters, Surf. Sci. 608 (2013) 129–134, https://doi.org/10.1016/j.susc.2012.09.024.
[46] H. Sa'Adeh, F. Backler, F. Wang, A. Ciavardini, S. Piccirillo, M. Coreno, R. Richter, K.C. Prince, An experimental and theoretical investigation of XPS and NEXAFS of nicotine, nicotinamide, and nicotinc acid, J. Phys. Conf. Ser. 1412 (2020). 10.1088/1742-6596/1412/10/102008.
[47] S. Ramalingam, S. Periandy, M. Govindarajan, S. Mohan, FT-IR and FT-Raman vibrational spectra and molecular structure investigation of nicotinamide: a combined experimental and theoretical study, Spectrochim. Acta - Part A Mol. Biomol. Spectrosc. 75 (2010) 1552–1558, https://doi.org/10.1016/j.saa.2010.02.015.
[48] M. Galli, S. Sáringer, I. Szilágyi, G. Trefalt, A simple method to determine critical coagulation concentration from electrophoretic mobility, Colloids Interf. 4 (2020) 20, https://doi.org/10.3390/colloids4020020.
[49] D. Huang, B. Ou, R.L. Prior, The chemistry behind antioxidant capacity assays, J. Agric. Food Chem. 53 (2005) 1841–1856, https://doi.org/10.1021/jf030723c.
[50] F. Xiao, T. Xu, B. Lu, R. Liu, Guidelines for antioxidant assays for food components, Food Front. 1 (2020) 60–69, https://doi.org/10.1002/fft2.10.
[51] G. Cao, H.M. Alessio, R.G. Cutler, Oxygen-radical absorbance capacity assay for antioxidants, Free Radic. Biol. Med. 14 (1993) 303–311, https://doi.org/10.1016/0891-5849(93)90027-R.
[52] S. Meziane, J. Magand, M. Mathé, S. Raimond, J. Yvon, M. Kaci, Bioavailability of natural and synthetic vitamins : A significant difference on Oxidative Stress Status (OSS), Integr. Food, Nutr. Metab. 8 (2021) 1–10. doi:10.15761/IFNM.1000301.